Modeling APL-Mediated Local Inhibition in the Fruit Fly Mushroom Body

Yijie Pan, Sachin Salim, Zhengxu Tang

December 2023
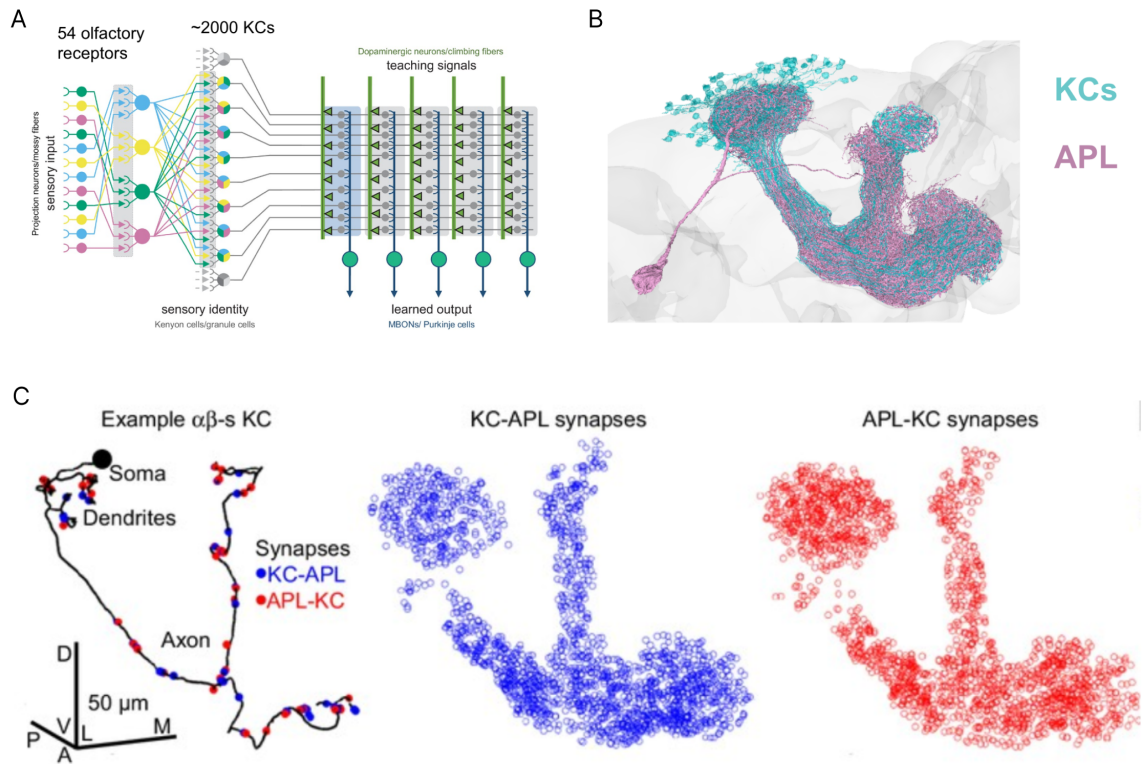
1 Background and Motivation

Figure 1: **Mushroom body is the associative learning center of insects:** A) Schematic structure of mushroom body-like neural network[9]. B) 3D mesh of 100 Kenyon Cells and a single APL from the flywire connectome. C). Synapses between KCs and APL from the connectome [1]. Left: Synapses on single KC. Blue dots are KC to APL excitatory synapses, and red dots are APL to KC inhibitory synapses. Middle: 2D projection of all KC to APL synapses. Right: 2D projection of all APL to KC synapses.

1.1 Background

The mushroom body, a pivotal neural structure, is recognized as the learning center in arthropods, encompassing a diverse range of species including insects, shrimps, and crabs. Remarkably, it shares a similar network architecture with key learning hubs in mammals, such as the cerebellum and hippocampus[3]. This commonality underscores a universal neural mechanism

underlying learning and memory across different phyla. In these neural hubs, a substantial population of neurons is engaged in processing combinatorial sensory inputs, leading to neuronal activity patterns that represent specific sensory contexts[11]. This mechanism is crucial for associating these sensory representations with corresponding behavioral responses, achieved through the modulation of synaptic strengths between representation neurons and their respective output neurons[5]. The critical factor in this process is the generation of sparse, minimally overlapping sensory representations within a large neuronal population, a feature essential for pattern separation and the accuracy of learning processes[3][6].

Focusing on the *Drosophila melanogaster* (fruit fly) mushroom body, which contains approximately 2000 Kenyon Cells (KCs), researchers have observed a unique input pattern where each KC receives inputs from a randomly selected subset of 54 olfactory channels (Figure 1 A). This intricate system is modulated by a giant GABAergic interneuron, known as the Anterior Paired Lateral (APL) neuron (Figure 1 B). The APL is instrumental in olfactory discrimination learning, receiving inputs from all KCs and in turn providing inhibitory feedback (Figure 1 C). Recent electrophysiological studies have revealed that the lateral inhibition from the APL is localized, affecting only a subset of KCs[7], contrary to previous beliefs of a more global inhibitory influence. This finding is further supported by transcriptomic studies suggesting that the APL's lack of voltage-gated channels for action potential generation could lead to localized inhibition[1]. This raises a fundamental question about how this localized inhibition contributes to the sparsity of sensory representations in the mushroom body.
Recent advancements in the field have illuminated the functionality of the APL, particularly its localized inhibitory impact on Kenyon Cells (KCs), a stark contrast to the previously assumed theories of widespread inhibition. This pivotal revelation raises intriguing questions regarding the role of sparsity in sensory representations and its consequent influence on learning efficacy. Especially noteworthy are the synaptic interactions between KCs and the APL neuron, as they potentially exert a significant impact on the transmission of sensory information to various output neurons.

1.2 Motivation

Prompted by recent findings and existing knowledge gaps, this study seeks to investigate the APL neuron's local inhibitory effects on sensory representations within the mushroom body. The foundation of this inquiry is the Kennedy-MB model, an amalgamation of multiple preceding models. However, this model's limitations include its assumption of uniform, global inhibition from the APL and a simplified depiction of KC dynamics(Figure 2)[8].

Our objective is to enhance this model by incorporating spatial relationships between KCs and implementing a more authentic Leaky-integrate and fire (LIF) model for KC dynamics. This enhanced model will facilitate a more precise exploration of local inhibition's implications on sensory representations.

Through this research, we aspire to enrich the understanding of local inhibitory mechanisms within the mushroom body and their bearing on sensory processing and learning in simpler neural systems. Our endeavor is to make substantial contributions to the broader comprehension of neural processing and learning mechanisms across both arthropods and mammals.

2 Model and Methods

2.1 Overview of the previous model: Kennedy-MB Model

The foundation of our computational approach is based on the Kennedy-MB model, developed by Ann Kennedy. This comprehensive simulation framework integrates multiple prior models to simulate neural processes from sensory input to Kenyon Cells (KCs) in the mushroom body. The input to the Kennedy-MB model comprises electrophysiology recordings of 23 types of olfactory receptor neurons (ORNs) responding to single odors from a 110-odor panel for 500 ms[4]. Projection neurons (PNs), which transmit signals from ORNs to KCs, are modeled using a Leaky-integrate and fire (LIF) mechanism, accounting for inputs from ORNs, spontaneous activity, and global inhibition from GABAergic local neurons (LN). The dynamics of PNs in the simulation are calibrated to match experimental results.
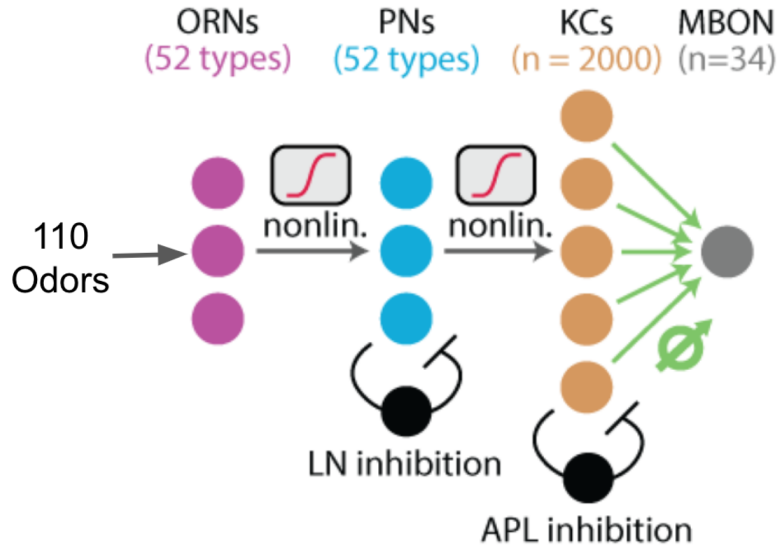

Figure 2: **Schematic of Kennedy-MB model[8].**

2.1.1 Simulation of Kenyon Cells Dynamics

In the Kennedy-MB model, KCs are represented using a simplified Leaky-integrate and fire model. The key parameters include:

$$\tau_m \frac{dV_m}{dt} = -V_m(t) + \sum_{i=1}^{n} w_i PN_i(t) - w_{APL}APL(t) \tag{1}$$

- V_m: Membrane potential of KCs, reset to default when reaching threshold θ.

- w: Synaptic weight (Connectivity) between PNs and KCs.

- PN: Excitatory input to KCs from PNs.

- APL: Inhibition from APL to KCs, modeled as a release of GABA.

$$\tau_m \frac{dAPL}{dt} = -APL + \sum_{i=1}^{N} KC_i \tag{2}$$

The model parameters include:

- *KC*: linear function of KC spikes.

APL integrates excitatory inputs from all KCs, with the release of GABA being a linear function of APL's membrane potential. The connectivity between PNs and KCs is modeled by randomly selecting 6 inputs from PNs, based on observed connectivity probabilities[2]. The firing threshold of KCs is tuned to achieve an average activity of 20% across a panel of odors, with inhibition strength adjusted to reduce the active KC population to 10%, reflecting experimental observations of APL's modulation of KC responses[10].

2.1.2 Modeling APL Inhibition

APL's inhibition is formulated as follows:

$$\text{APL Inhibition} = \alpha \times \sum_{i}^{N_{KC}} \text{KC}_i \tag{3}$$

where α is a scaling factor and N_{KC} is the number of KCs.

2.1.3 Numerical Implementation

The numerical implementation of the Kennedy-MB model involves simulating the dynamics of the KCs under varying sensory inputs and inhibition levels. This implementation utilizes the following steps:

1. Electrophysiological data of ORNs responding to different odors are inputted into the model.

2. The response of PNs is simulated based on inputs from ORNs, accounting for spontaneous activity and global inhibition.

3. KC dynamics are simulated using the LIF model parameters, incorporating inputs from PNs and inhibition from APL.

4. The model's output is analyzed to assess the sparsity of sensory representations and the impact of APL's inhibition on KCs.

2.2 Modeling Kenyon cells as 2D matrix

For the convenience of implementation, we use a 45×45 matrix to represent 2025 KCs. Given that KCs' dendrites are distributed in a relatively parallel and unifrom manner[12], this matrix successfully abstracts the spatial relationships between all KCs. The excitatory presynaptic neurons of KCs is called projection neurons (PNs). In Kennedy-MB model, each KC randomly connects to 6 PNs and receives inputs from them. We followed this strategy to simulate inputs to KCs (Figure 3 A), and improve the simulation of connectivity to mimic real physiological conditions in real brains.
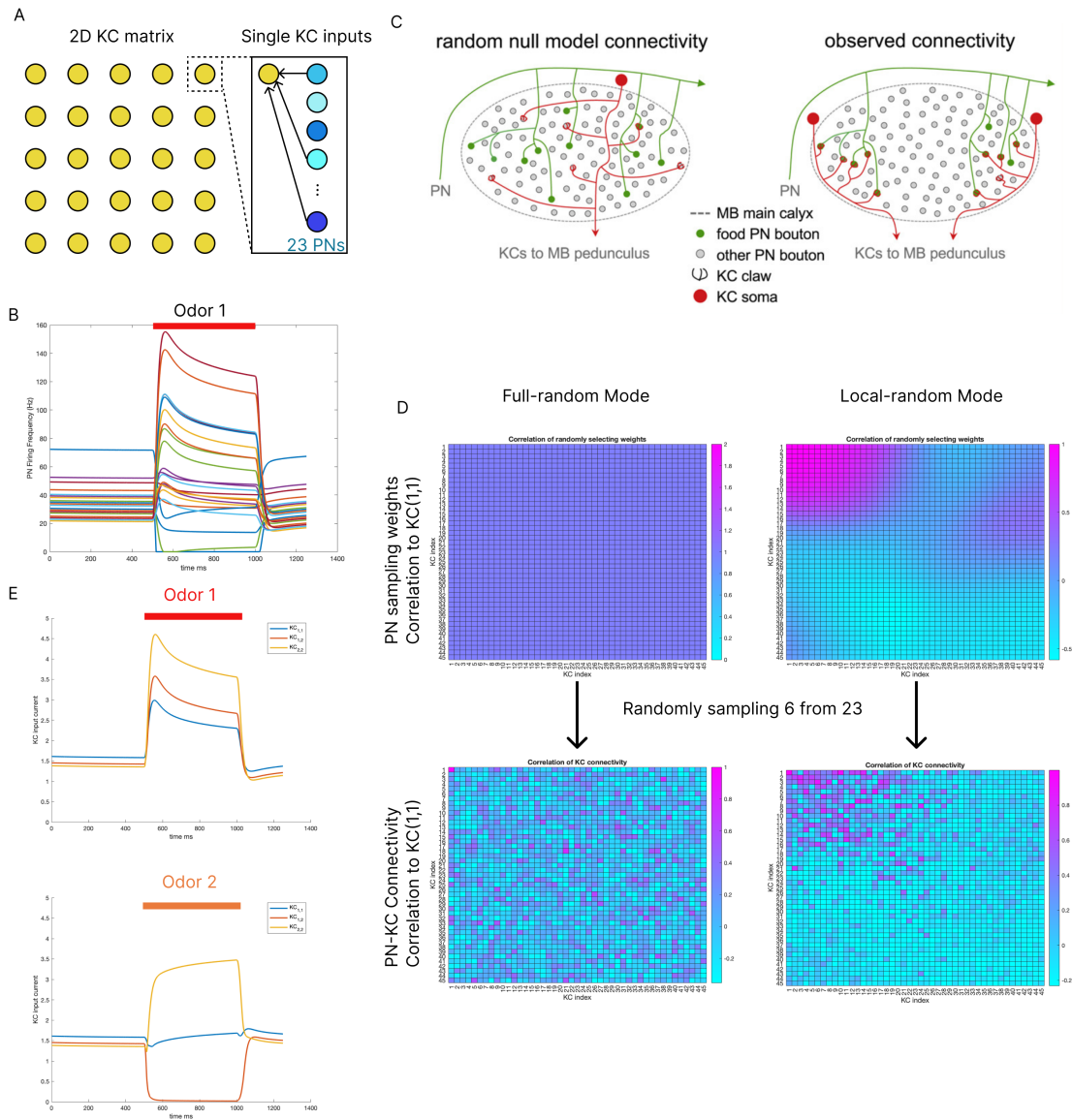
Figure 3: **Modeling the input of Kenyon Cells:** A) Schematic structure of 2-D Kenyon Cell (KC) matrix. We use a 2-D matrix to abstract the spatial relationships between KCs. Each KC in the matrix randomly connect with 6 out of 23 Projection Neurons (PN). B) The firing frequency of 23 Projection Neurons responding to odor 1 simulated in Kennedy-MB model. Those 23 PNs are simulated based on real experimental recording on corresponding sensory neurons. C) Observations from the connectome data shows there are spatial constraints for the connections from PNs to KCs. KCs are likely to randomly receive inputs from PNs who have axon boutons around them[12]. D) Examples of different connectivity modes. In Kennedy-MB model, each KC randomly sample inputs from PNs with even weight, which is named "Full-radom Mode". To simulate the connection with spatial constrains, for each PN we randomly assigned some connecting "Hot Spots" on the KC matrix, that at those hot spots, KCs have higher sampling weight to this PN. The upper heatmaps show the similarity of sampling weights of all KCs to the KC on upper left corner. The lower heatmaps show the similarity of all KC-PN connectivity to the upper left corner KC after random sampling. E) Examples of inputs KCs receiving.

2.2.1 KC inputs

We extracted the odor responses of PNs from the Kennedy-MB model. 23 out of 51 PNs are simulated from experimental recordings of corresponding ORNs, thus we only extracted odor response from these PNs. For each PN, the odor responses are simulated by adding the odor triggered increase of firing rate to the spontaneous firing rate (Figure 3 B). Odor stimuli is from 500 ms to 1000 ms since the start of simulation.

It is believed that the connections between PN and KC is completely random[2] (Figure 3 C, left). We simulated this scenario by randomly sampling 6 inputs from 23 PNs with replacement, as in nature it is possible for each KC to connect with the same type of PNs multiple times. For n-th PN, we defined a sampling weight matrix as the same size of KC population, $SampleW_n(n \in [1, 23])$. For $KC_{i,j}(i, j \in [1, 45])$, its connected PN is randomly sampling based on the weights $SampleW_{i,j,1:23}$, in which n is the PN index, and i and j are the KC position indices. After we sample the connected PNs for all KCs, we will get the binary PN-KC connectivity matrix wPN. If there is no spatial constrains, all PNs at every KC position has equal weight to be connected. We name this connectivity mode as "Full-random mode" (Figure 3 D, left). With this connectivity mode, KCs having similar connectivity are scattered in the 2-D KC matrix. However, recent analysis from the connectome data suggests that there are spatial constraints for PN-KC connectivity, that spatially close KCs are likely to receive similar inputs from PNs [12] (Figure 3 C, right). To simulate this scenario, for each PN we randomly select "connectivity hotspots" at $[m, n](m, n \in [1, 45])$. We assigned the PN-KC sampling weight following 2D normal distributions centered at those connectivity hotspots, and randomly sampled 6 from 23 PNs with replacement based on the assigned weights at corresponding KC position. This connectivity mode is named "Local random mode". With this mode, KC spatially close to each other will have higher chance to sample from PNs with similar weight, and end up with similar connectivity (Figure 3 D, right).

We assume the inputs KCs receive from PNs are instantaneous and linearly correlate with PNs firing rate. For $KC_{i,j}$, the input current is:

$$I(t)_{i,j} = A \cdot wPN_{i,j} \times PN(t) \tag{4}$$

In which $I(t)_{i,j}$ is the input current for $KC_{i,j}$ at time step t, A is a linear scale factor, $wPN_{i,j}$ is the connectivity between $KC_{i,j}$ and 23 PNs, and $PN(t)$ is the firing frequency of 23 PNs at time step t. The examples of heterogeneous KC inputs are shown (Figure 3, E).

2.2.2 KC dynamics

Each Kenyon Cell is implemented as a 2D LIF Izhikevich model. We followed the below equations and parameters:

$$\frac{dV}{dt} = 0.04V^2 + 5V + 140 - u + I_{app}$$

$$\frac{du}{dt} = a(bV - u)$$

Reset condition: If $V \geq 30$, then set $V = c$ and $u = u + d$
Parameter values: $a = 0.02$, $b = 0.2$, $c = -65$, $d = 8$
For odor 1, the input current to KC and the respective firing rates is visualized in Figure 4 for a disconnected network. A comparison is also considered between Full-random and Local-random mode. This helps in speculating the variation of input current among KCs and how this affects the firing rate.
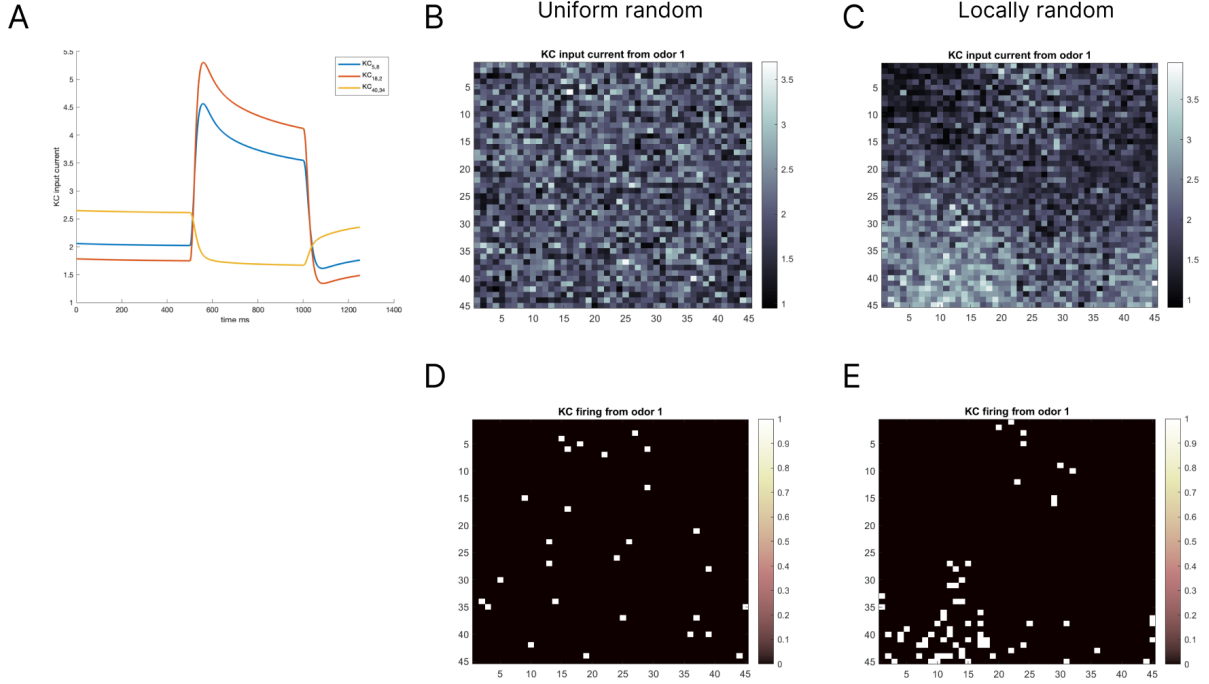
Figure 4: **Uniform v/s local sparsity.** A) Input currents for odor 1 visualized for three sample KC. B, C) Input currents (max) visualized as a raster plot for all KC for uniform and local connectivity. D, E) The output firing rate of KC in a disconnected network

2.3 Modeling local inhibition of APL

As explained in the previous sections, the Kenyon Cells are implemented as 2D LIF models in a 2D network. The next step in the modelling is to incorporate the inhibition of KCs from APL. As seen from the physiological data, APL performs local inhibition to KCs. This local forward/feedback inhibition of APL is modeled as a local lateral inhibition among Kenyon cells. Since the inhibition effect from a particular is prominent in its local neighborhood and decrease as a function of distance, the connection weight of a presynaptic-KC to a postsynaptic KC is modeled to decay with distance. We modeled this relationship as a gaussian function.

$$w_{syn}(r) = \exp\left(-\frac{r^2}{2\sigma^2}\right)$$

See Figure 5 for a detailed visualization of how the connectivity is modelled.

2.4 Model evaluation

2.4.1 Responding fraction

We use responding fraction to estimate the sparsity of odor triggered KC responses. The responding fraction F for a given odor stimulus is calculated as:

$$F_{odor_i} = \frac{n_{odor_i}}{N} \tag{5}$$

In which n_{odor_i} is the number of KCs have at least one spike for stimulus $odor_i$, and N is the total KC number (N=2025 in this project).
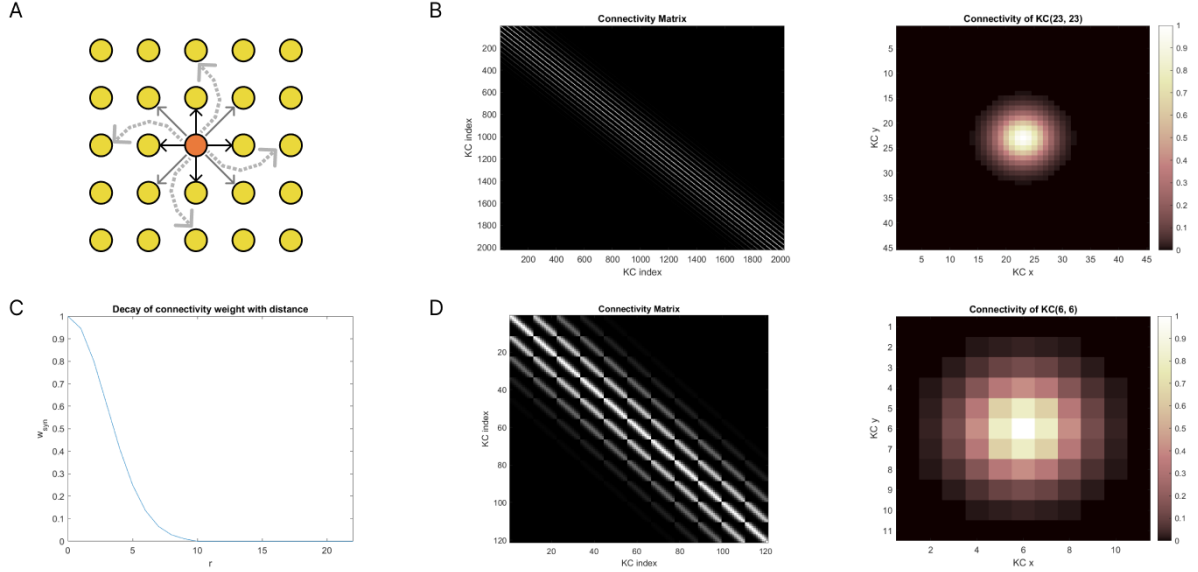
Figure 5: **Connectivity matrix of KC cells.** A) This figure illustrates how KC cells are connected in a 2D grid. The center cell (orange) is connected to all its neighboring cells but the strength decays with distance. B) Adjacency matrix showing how the KC cells are connected (n=2025 [45x45], $\sigma = 3$) C) Plot showing the connectivity strength decaying with spatial distance. D) Adjacency matrix of a smaller network for visualization purpose (n=121 [11x11], $\sigma = 1.5$)

2.4.2 Lifetime sparseness

We use the same method as in Kennedy-MB model to precisely quantify sparseness of KC activity. The sparseness S a given odor stimulus is calculated as:

$$S_{odor_i} = (1 - (\frac{(\sum_{i=1}^{KC_{d1}} \sum_{j=1}^{KC_{d2}} r_{i,j}/N)^2}{\sum_{i=1}^{KC_{d1}} \sum_{j=1}^{KC_{d2}} r_{i,j}^2/N}))/(1 - \frac{1}{N}) \tag{6}$$

In which $r_{i,j}$ is the spike counts for $KC_{i,j}$, KC_{d1} and KC_{d1} are the two dimensions of 2-D KC matrix (45 in this project), and N is the total KC number (N=2025 in this project). The more S_{odor_i} is close to 1, the sparser responses are. See Figure 6 for a visual analysis of how the sparseness S is affected by varying the inhibition parameters.

2.4.3 ROC curve

To compare the linear separability of odor representations in KC layer, we construct a linear classifier to separate the odor representations, and compare the performace of different models using ROC curve.

The linear classifier processes odor representations as following steps:

- We set the original simulated odor responses in KCs are the "ground truth".

- We add non-negative gaussian noise with $\sigma = 0.5$ to the simulated odor responses to mimic realistic odor representation of odors with background noise. This is named as testing odors as stated below.

- For each original odor response $Odor_i$, we calculated its Euclidean distance to all testing odors and normalize the distances to $[0, 1]$ by Min-Max normalization. For a given threshold th, if the normalized distance from the testing odors are smaller than th, we classify
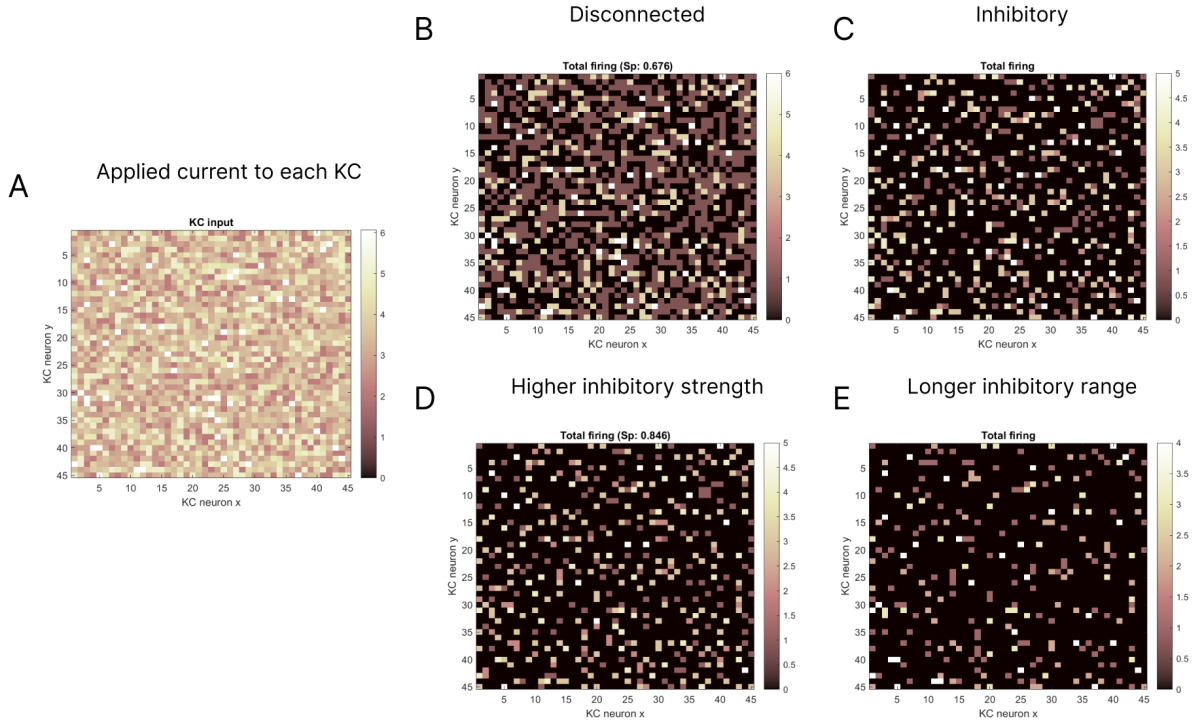
Figure 6: **Inhibition affects Sparsity.** These figures visualize how varying inhibition strength and range affects the sparsity of KC firing. Analysed for odor 1, full random, A = 0.035, taus = 50. A) visualizes the maximum input current across the time for each of the KC cells. B) gsyn = 0 ↦ sparseness: 0.676 C) gsyn = -2, σ = 1 ↦ sparseness: 0.822 D) gsyn = -5, σ = 1 ↦ sparseness: 0.846 E) gsyn = -2, σ = 3 ↦ sparseness: 0.912

these odors are $Odor_i$. The counts for true positive TP (testing $Odor_j$ is classified as $Odor_i$, $i = j$), false positive FP (testing $Odor_j$ is classified as $Odor_i$, $i \neq j$), true negative TN (testing $Odor_j$ is not classified as $Odor_i$, $i \neq j$) and false negative FN (testing $Odor_j$ is not classified as $Odor_i$, $i = j$).

- We gradually change the value of th from 0 to 1, and keep track TP, FP, TN, FN for each threshold.

To plot the ROC curve, we calculate the true positive ratio TPR and False positive ratio FPR as:

$$TPR = \frac{TP}{TP + FN} \tag{7}$$

$$FPR = \frac{FP}{FP + TN} \tag{8}$$

A ROC curve for a model plots TPR vs. FPR with different classification thresholds. The models with overall higher TPR and lower FPR have better linear separability.

3 Results

3.1 Local inhibition increases odor separability

In our 2-D grid KC model, each KC receives excitatory inputs from PNs, the strength of which is regulated by parameter A, and inhibitory inputs from other KCs, implemented with a negative $gSyn$ value. From previous literature, odor representation sparseness is critical for the animal's

ability to discriminate similar odors [10] (Figure 7 A). Following the Kennedy-MB model, we initially adjust the input strength parameter A to achieve 25% KCs responding to randomly selected odors without inhibition (Figure 7 B).

To explore the effect of local inhibition strength on KC odor response sparseness, with fixed input strength and inhibition range $\sigma = 10$, we measured the averaged lifetime sparseness and responding fraction with $gSyn \in [-0.25, 0]$ (Figure 7 C, D). As $gSyn$ becomes more negative, the lifetime sparseness increases with inhibition strength and converges towards 1. The responding fraction of KCs also quickly drops and converges towards a minimum value. Changing the connectivity mode from full-random mode to local random mode doesn't affect sparseness. Notably, the variance of sparseness and responding fraction decreases with stronger inhibition strength, indicating that local lateral-feedback inhibition can normalize odor responses. In other words, odors that trigger responses in more KCs are likely to be more affected by inhibition.

Similar to the global inhibition in the Kennedy-MB model that increases sparseness, we tested whether local inhibition can increase odor separability using ROC curve analysis (Figure 7 E, F). In both full-random connectivity mode and local-random connectivity mode, stronger inhibition has better odor representation separation performance. Strikingly, the local-random connectivity mode shows better performance even without any inhibition compared to full-random connectivity. In both connectivity modes, the number of odors to which no KC responds does not increase with inhibition strength (data not shown).

3.2 Odor separability are robust to change of inhibition range

In the previous section, our results show that local inhibition can sparsen odor responses in KCs and increase their separability. Next, we want to test the effect of the inhibition range on odor responses in KCs. Given the large inhibition range, each KC receives more inhibitory inputs, and the $gSyn$ value needs to be tuned for the corresponding inhibition range to eliminate this confounding factor. For a series of inhibition ranges $\sigma \in [0, 100]$ (when $\sigma > 50$, it is implemented as global inhibition, and when $\sigma = 0$, it is implemented as no inhibition), we mapped the corresponding $gSyn$ values to achieve an average responding fraction of 10%, consistent with the Kennedy-MB model (Figure 8 A). These results suggest that local inhibition can achieve the same sparseness as global inhibition models with stronger inhibition strength.

We applied the mapped parameters to the entire 110-odor response dataset and validated that the sparseness and responding fraction are the same for models with different inhibition ranges (Figure 8 B, C). Using the ROC curve, we compared the odor separation performance. In the full-random connectivity mode, models with different inhibition ranges have comparable performance (Figure 8 D). Interestingly, in the local-random connectivity mode, the performance increased with the inhibition range(Figure 8 E).
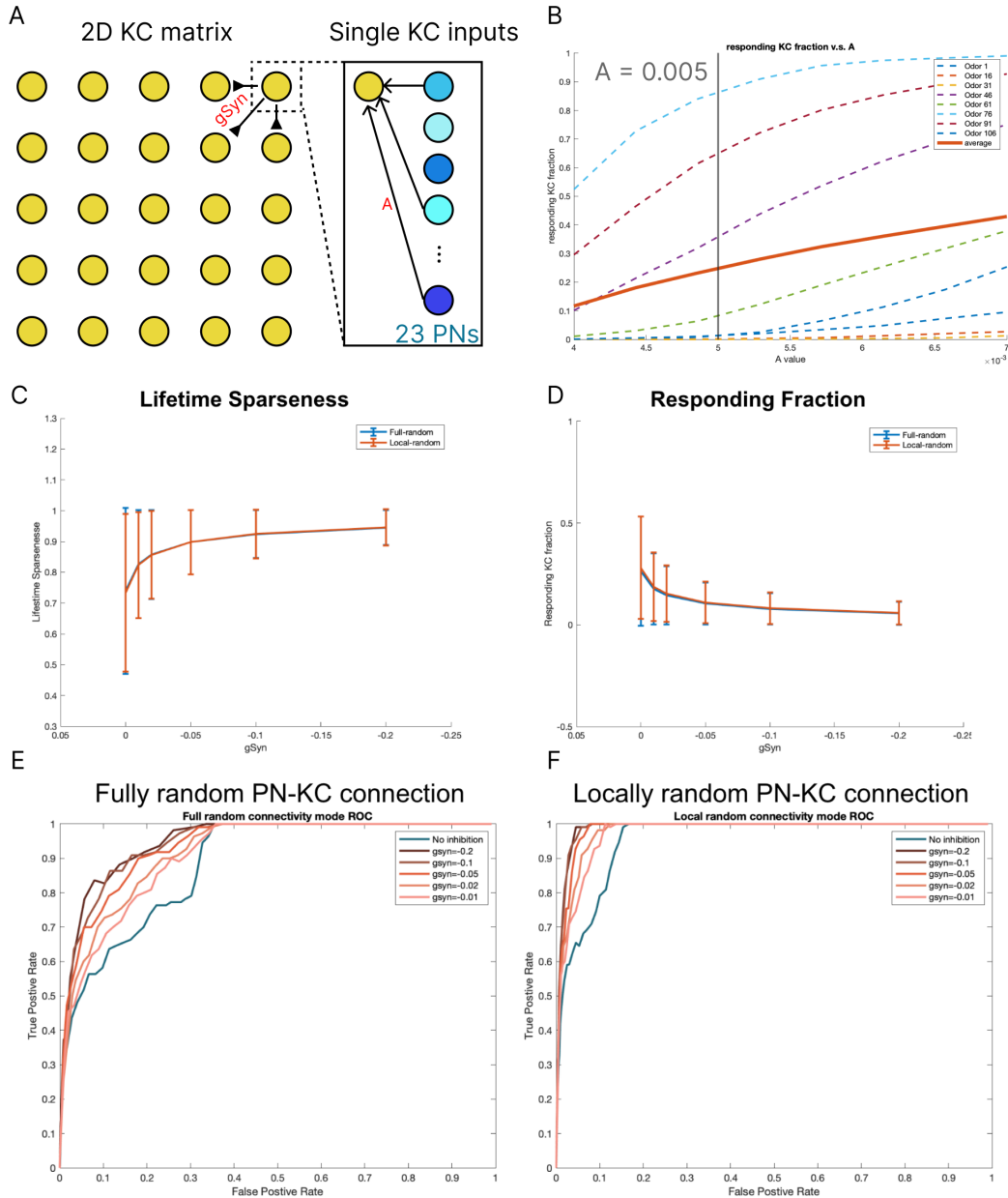
Figure 7: **Local inhibition increases odor separability:) A) The diagram of tuned parameters.** A **is input strength, which linearly scale the input from PN to KC;** $gSyn$ **is the inhibition strength, which r**gulate the amplitude of inhibition current from APL to KCs. B) Fit input strength to Kennedy-MB model. When $A = 0.005$ and no inhibition from APL, the averaged resounding fraction of 8 randomly selected odors is 25%. C) The 110 odors' averaged lifetime sparsenesses of both full-random connectivity mode and local-random connectivity mode are increased with the inhibition strength $gSyn$. D) The 110 odors' averaged responding fraction of both full-random connectivity mode and local-random connectivity mode are decreased with the inhibition strength $gSyn$. E) The ROC curve of full-random connectivity models with different inhibition strength. Models with stronger inhibition strength have better classification performance. F) The ROC curve of local-random connectivity models with different inhibition strength. Models with stronger inhibition strength have better classification performance. (The models from C to F are simulated with $A = 0.005$, $\sigma = 10$).
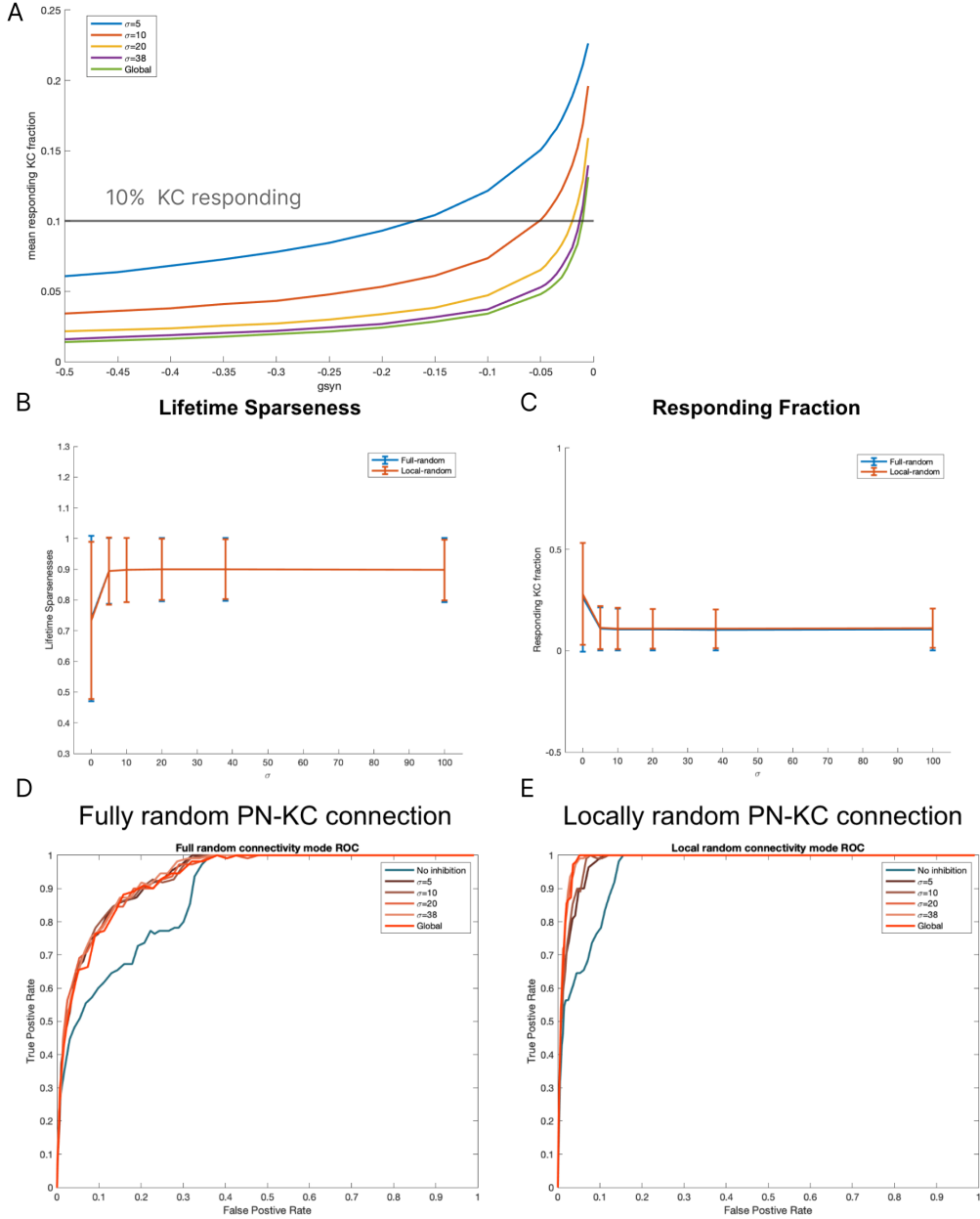
11

Figure 8: **Odor separability are robust to change of inhibition range:** A) To control the sparsity and vary inhibition range σ, the inhibition strength is adjusted to let the averaged averaged resounding fraction of 8 randomly selected odors archive 10%. B) The averaged lifetime sparsenesses of 110 odors simulated with models with different inhibition range and corresponding adjusted inhibition strength. When the inhibition range $\sigma > 50$, it is implemented as global inhibition that all KCs inhibit other KCs equally. C) The averaged responding fractions of 110 odors simulated with models with different inhibition range and corresponding adjusted inhibition strength. D) The ROC curve of full-random connectivity models with different inhibition range and corresponding adjusted inhibition strength. In this connectivity mode, changing inhibition range only do not affect the classification performance. E).The ROC curve of local-random connectivity models with different inhibition range and corresponding adjusted inhibition strength. In this connectivity mode, models with smaller inhibition range shows relatively decreased classification performance.(The models are simulated with $A = 0.005$)

4   Summary and Conclusions

Recent findings suggest that local inhibition, a more realistic mechanism, exhibits comparable effectiveness to global inhibition models in regulating the sparsity of Kenyon cell (KC) outputs. Stronger inhibition intensifies sparsity, enhancing the distinctiveness of odor representations. Consequently, this heightened separability enables animals to discern the source odor with greater accuracy. Interestingly, altering the sparsity control and adjusting the inhibition range showcases no significant impact on prediction performance in scenarios featuring full random connectivity between projection neurons (PNs) and KCs. However, models incorporating local-random PN-KC connectivity exhibit enhanced performance compared to those employing uniform or full random connectivity. Simulation results substantiate the superiority of physiologically realistic models in predicting odors, elucidating the evolutionary advantage underlying their existence.

4.1   Comparison between local inhibition and global inhibition

In our simulation, with stronger inhibition strength, local inhibition has the same performance as global inhibition, as long as the sparseness of odor responses is the same. Given the limited spatial-temporal information on how the actual APL integrates its inputs from KCs and provides inhibition, we couldn't explicitly simulate APL. However, our results suggest that a physiologically reasonable localized inhibition in the KC layer is functional and potentially validates the results regarding sparseness and odor separation performance of previous models based on global inhibition.

4.2   Augmented performance with local-random connectivity mode

Our results show that the local-random connectivity mode has better performance in terms of odor separation ability. We hypothesize that with the local-random connectivity model, the distribution of PN-KCs connectivity already separates the representation in the KC layer spatially, thereby locally reducing the redundancy of using 2000 cells to encode 110 odors. In other words, for the odor responses to those disliked odors, they are already separated and represented by a different set of KCs. There might be a trade-off, where the representations of similar odors might overlap more in this connectivity mode. We need to further validate this by comparing the spatial distribution of odor representation and inter-odor correlations when we have more time.

5   Responses to Questions

5.1   Question 1

How did you decide on a gaussian kernel for your connectivity? Do you have any guesses for what might happen with different shapes (center-surround, exponential cutoff, etc.)? Also, can you explain in more detail how different scents are modeled?
Answer: The concept of center-surround organization, which induces sparsity by exciting a neuron's self and inhibiting its neighbors, seemed promising. However, analyzing physiological data revealed that kenyon cells not only inhibit their neighbors via APL, but they also receive inhibition themselves due to feedback inhibition from APL. This finding suggests that the center-surround model might not accurately reflect the biological reality. In our investigation, we opted for a Gaussian decay function (e^{-x^2}) over an exponential cutoff function (e^{-x}). This choice was driven by the intent to emulate a high inhibition strength within the local neighborhood, and then steeply taper off at a distance. This modeling approach aligns more closely with the

observed connectome data, providing a better representation of the neural network's inhibitory patterns.

There are approximately 51 types of distinct olfactory receptors and corresponding sensory neurons. In 2006, a large-scale single-unit electrophysiology recording experiment mapped responses from 23 types of olfactory sensory receptor neurons to an odor panel consisting of 110 odors [4]. The direct downstream neurons of olfactory sensory neurons are called projection neurons. For each type of olfactory sensory neuron, there are corresponding projection neurons specifically receiving inputs from them. In the Kennedy-MB model, the activity of projection neurons is modeled by a firing rate model that takes the experimental recordings on sensory neurons as inputs. The simulated projection neurons have been validated and match other experimental measurements. In our model, we inherited the simulated projection neuron responses to 110 odors from the Kennedy-MB model, and our modeled Kenyon cells (KCs) receive combinatory inputs from 23 types of projection neurons.

5.2 Question 2

How could this model be used or what might have to be modified to represent impairment of the olfactory system?

Answer: This model can represent three levels of impairment in the olfactory system:

1. Olfactory Receptor Mutations: If there are mutations in olfactory receptors, and the affected receptors are among the 23 mapped types, we can suppress the mutated sensory channel and examine how the alteration influences odor discrimination ability.

2. Variability in Kenyon Cell Numbers: The number of Kenyon cells can vary significantly based on mutation conditions, developmental temperatures, and genetic defects. In our model, considering both the number of Kenyon cells and their spatial relationships, we can assess how changes in Kenyon cell numbers alter odor discrimination ability.

3. Mammalian Olfactory System Simulation: The mammalian olfactory system exhibits a similar topological structure to the mushroom body, but the connections between neurons are more plastic. By adding more layers of Kenyon cells and updating their connections following Spike-Timing-Dependent Plasticity (STDP) rules, we can simulate the piriform cortex in mammals. This allows us to test how defects in inhibitory interneurons and changes in the electrophysiological properties of excitatory neurons alter odor representations.

6 References

[1] Hoger Amin, Anthi A Apostolopoulou, Raquel Suárez-Grimalt, Eleftheria Vrontou, and Andrew C Lin. Localized inhibition in the drosophila mushroom body. *Elife*, 9:e56954, 2020.

[2] Sophie JC Caron, Vanessa Ruta, Larry F Abbott, and Richard Axel. Random convergence of olfactory inputs in the drosophila mushroom body. *Nature*, 497(7447):113–117, 2013.

[3] N Alex Cayco-Gajic and R Angus Silver. Re-evaluating circuit mechanisms underlying pattern separation. *Neuron*, 101(4):584–602, 2019.

[4] Elissa A Hallem and John R Carlson. Coding of odors by a receptor repertoire. *Cell*, 125(1):143–160, 2006.

[5] Annie Handler, Thomas GW Graham, Raphael Cohn, Ianessa Morantte, Andrew F Siliciano, Jianzhi Zeng, Yulong Li, and Vanessa Ruta. Distinct dopamine receptor pathways underlie the temporal sensitivity of associative learning. *Cell*, 178(1):60–75, 2019.

[6] Toshihide Hige, Yoshinori Aso, Mehrab N Modi, Gerald M Rubin, and Glenn C Turner. Heterosynaptic plasticity underlies aversive olfactory learning in drosophila. *Neuron*, 88(5):985–998, 2015.

[7] Kengo Inada, Yoshiko Tsuchimoto, and Hokto Kazama. Origins of cell-type-specific olfactory processing in the drosophila mushroom body circuit. *Neuron*, 95(2):357–367, 2017.

[8] A Kennedy. Learning with naturalistic odor representations in a dynamic model of the drosophila olfactory system. biorxiv 783191, 2019.

[9] Feng Li, Jack W Lindsey, Elizabeth C Marin, Nils Otto, Marisa Dreher, Georgia Dempsey, Ildiko Stark, Alexander S Bates, Markus William Pleijzier, Philipp Schlegel, et al. The connectome of the adult drosophila mushroom body provides insights into function. *Elife*, 9:e62576, 2020.

[10] Andrew C Lin, Alexei M Bygrave, Alix De Calignon, Tzumin Lee, and Gero Miesenböck. Sparse, decorrelated odor coding in the mushroom body enhances learned odor discrimination. *Nature neuroscience*, 17(4):559–568, 2014.

[11] Liqun Luo. Architectures of neuronal circuits. *Science*, 373(6559):eabg7285, 2021.

[12] Zhihao Zheng, Feng Li, Corey Fisher, Iqbal J Ali, Nadiya Sharifi, Steven Calle-Schuler, Joseph Hsu, Najla Masoodpanah, Lucia Kmecova, Tom Kazimiers, et al. Structured sampling of olfactory input by the fly mushroom body. *Current Biology*, 32(15):3334–3349, 2022.

7 Code Summary

The project was entirely coded in MATLAB and hosted in our GitHub repository. To generate 23 PN odor responses as input to our KC models, we modified the code written by Ann Kennedy for Kennedy-MB model. The matlab code of Kennedy-MB model is open sourced in Ann Kennedy's GitHub repository. The modified version is available upon request. To model the dynamics of Kenyon Cells as a 2D LIF Izhikevich model, we made use of the `LIF2D_simple_network.m` code provided in class. We independently developed the 2D network structure and the decay of connection weights from scratch. In addition to implementing the computation of sparsity, we authored the visualization tools and evaluation code, including ROC calculation methods. The full codes can be acquired from our team members.